

Accepted version on Author's Personal Website: C. R. Koch

Article Name with DOI link to Final Published Version complete citation:

H. Babazadeh, C. R. Koch, and D. S. Nobes. Investigation of micro-jet active control of a precessing jet using PIV. *Experiments in Fluids*, 51:1709–1719, 2011. ISSN 0723-4864. doi: [10.1007/s00348-011-1193-0](https://doi.org/10.1007/s00348-011-1193-0)

See also:

https://sites.ualberta.ca/~ckoch/open_access/babazadeh_piv_2011.pdf

Post-print

As per publisher copyright is ©2011



This work is licensed under a
[Creative Commons Attribution-NonCommercial-NoDerivatives 4.0 International License](#).



Article accepted version starts on the next page →
[Or link: to Author's Website](#)

Investigation of Micro-jet Active Control of a Precessing Jet using PIV

Hamed Babazadeh · Charles Robert Koch · David S. Nobes

Received: 10 March 2011 / v3h

Abstract A circular jet entering an open ended concentric circular chamber can rotate or precess about the jet axis for certain flow conditions and chamber configurations. Active flow control of a precessing jet provides the ability to influence the flow field inside the chamber and the resulting flow after the chamber exit. Twelve micro-jets surrounding the jet at the chamber inlet are used as actuation. At the chamber exit, four pressure probes and three component velocity measurement using stereo particle image velocimetry (stereo-PIV) is used to monitor the flow. A phase plane method using signals from the pressure sensors is developed to monitor the location of the jet high velocity region in real-time. Phase-locked stereo-PIV, triggered by the micro-jet actuation signal, is used to investigate the flow field and validate the pressure phase plane results. The effectiveness of the micro-jet actuation and the validation of the pressure phase plane measurements demonstrate actuation and sensing needed for future closed loop control of the precessing jet.

Keywords Precessing jet · Active flow control · Phase plane · Stereo-PIV · Jet actuation · Real time monitoring

Hamed Babazadeh
E-mail: babazade@ualberta.ca

Charles Robert Koch
E-mail: bob.koch@ualberta.ca

David S. Nobes
Department of Mechanical Engineering
University of Alberta
Edmonton, AB Canada T6G 2G8
E-mail: david.nobes@ualberta.ca

1 Introduction

Flow control in fluid mechanics refers to the manipulation of a flow field in order to alter the flow towards a desired state (Gad-el-Hak, 2006). The objectives of flow control vary from drag reduction in airplanes to mixing enhancement in industrial burners (Gad-el-Hak, 2006; King et al, 2010). Flow control is often classified into two major categories which are based on whether auxiliary power is used for actuation (active) or not (passive) (Gad-el-Hak, 2006). Manipulation of a turbulent free jet using different nozzle shapes is an example of passive control (Mi and Nathan, 2009). Using pulsed micro-jets around an axisymmetric jet to alter its near field mixing is an example of active flow control (Behrouzi et al, 2008).

For active flow control it is essential to have effective actuation (controllability) and be able to measure the phenomena of interest (observability). To achieve controllability, the actuation system must be strong enough to manipulate the main flow but the actuation should not be such a strong secondary flow that it changes the nature of the main flow. If the flow has a natural hydrodynamic instability this can provide a means to control the flow by adding only a small amount of energy. A self-excited unstable jet flow, referred to as a *precessing jet*, is the focus of this work and is combined with active flow control. Flow systems that develop the precessing jet phenomenon are used in industrial scale burners for the production of lime and cement (Nathan et al, 2006). The rotational motion causes a significant increase in entrainment rate and radiant heat transfer which result in a significant reduction in NO_x emissions (up to 70%), considerable fuel saving (up to 20%) and an improvement in product quality (up to 10%, e.g. in the lime industry) (Manias et al, 1996).

A schematic representation of the nozzle used to generate a precessing jet is shown in Figure 1. This nozzle consists of an axisymmetric jet with a nozzle inlet diameter of d discharging through a sudden expansion into a confined chamber with a length of L and a diameter of D such that $\frac{D}{d} = 5$. Precession occurs as the jet from the nozzle reattaches asymmetrically to part of the chamber inner wall and rotates about the nozzle axis. The flow, now a wall jet, is deflected across the chamber axis on leaving the chamber due to an exit lip. Flow visualization techniques both in air and water have shown that the precessing jet reattaches to the chamber wall about halfway down the chamber length (Nathan et al, 1998). A lip is often mounted at the chamber exit to assist the deflection as the jet exits the chamber. The deflection angle between the precessing jet and the chamber axis is 50° and decreases to 30° at $Z = 0.4D$ downstream of the chamber outlet plane (Wong et al, 2003)

Two different modes have been observed for this nozzle configuration, a precessing mode and an axial mode (Nathan et al, 1998). In *precessing mode*, the flow leaving the chamber rotates or spins (precesses) around the chamber axis as it exits the chamber. In *axial mode*, the jet exits the chamber uniformly in the axial direction as an axisymmetric jet. These two modes can be interspersed in time and the fraction of time in precessing mode is referred to as the probability of precession (Nathan et al, 1998). The precessing mode can be further divided into two flow regimes. In the first regime, the jet precesses regularly around the chamber axis. In the second regime, the flow does not complete a precessing cycle around the centerline, but rather jumps among a few locations along the chamber wall. The precessing jet experiences an unstable state in each mode and arbitrarily switches between them (Guo et al, 2001). A geometric ratio range in which precession occurs has been found to depend on the chamber geometry ($2 \leq \frac{L}{D} \leq 3.5$) (Nathan, 1988; Newbold, 1998).

The effect of chamber length on the jet precessing probability has been investigated and shows that the highest probability occurs in a range of $2 \leq \frac{L}{D} \leq 2.75$ but further increase of the length ratio results in a significant drop in the probability of precession (Madej et al, 2011). A passive control approach using geometric modifications to the chamber have been used to stabilize the precessing mode. For example, the addition of a baffle or a center body at the chamber exit, decreases the probability of the axial mode while stabilizing the precessing mode (Wong et al, 2004). The use of a triangular rather than circular jet nozzle has also been found to increase the probability of the precessing mode (England et al, 2010).

The precession instability is sensitive to variations in the initial and boundary conditions which is desirable since the flow can be controlled with a low level of input energy (Wong et al, 2004). The interaction of the jet with the chamber appears to make the precessing jet flow absolutely unstable (Huerre and Monkewitz, 1985) inside the chamber making it amenable to feedback control. The aim of the current study is to determine the ability of micro-jet actuation to stabilize precession (controlability) and the use of pressure sensors at the chamber exit to determine the flow mode (observability). This understanding will allow the development of active flow control strategies in future work.

2 Experimental methods

2.1 Experimental setup and facility

A schematic view of the precessing jet nozzle configuration used in the flow experiments is shown in Figure 1. A closed-loop flow system circulates room temperature

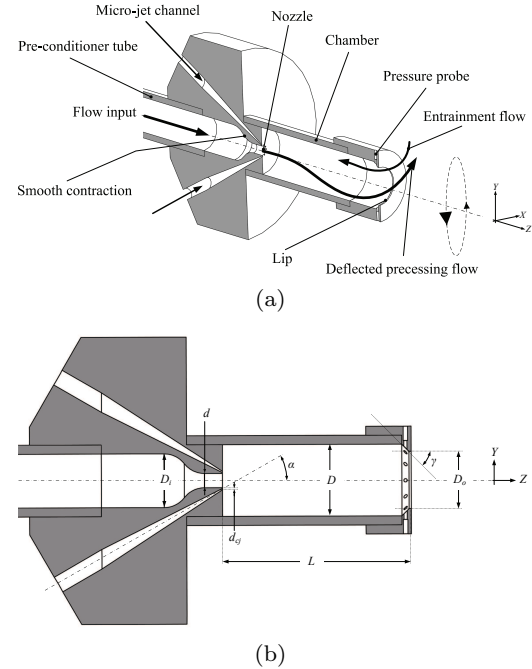


Fig. 1: (a) A schematic view of the nozzle and chamber setup (b) Section of the precessing jet with the lip including the 12 micro-jet actuation injection ports and the 4 pressure probes. $\frac{L}{D} = 2.5$, $\frac{D}{d} = 5$, $\frac{D_o}{D} = 0.8$, $\frac{D_i}{D} = 0.75$, $\frac{d_{cj}}{d} = 0.1$, $\alpha = 30^\circ$ and $\gamma = 45^\circ$.

water as the working fluid through the precessing nozzle. The water is driven by a progressive cavity pulseless

pump (Model 33204, Moyno) whose speed is set manually by a variable frequency drive. The output from the pump passes flow through a flowmeter for bulk characterization and into a flow plenum that feeds the precessing nozzle. The plenum consists of a settling chamber, four stages of grid plates and a honeycomb grid that have been designed to generate a uniform flow profile with low flow fluctuations and no swirl. A smooth contraction at the end of the plenum is connected to the pre-conditioner pipe (200 mm long) shown in Figure 1(a) that directly feeds the nozzle $d = 5.08$ mm providing a uniform and low fluctuation inlet condition into the precessing nozzle.

The axisymmetric chamber used, has a diameter of $D = 25.4$ mm and is directly coupled onto the inlet nozzle. The important dimensionless relationships for the precessing jet are given in Figure 1(b) with $\frac{L}{D} = 2.5$ and $\frac{D}{d} = 5$ chosen to ensure that precession occurs. The Reynolds number of the precessing jet is defined using the diameter of the axisymmetric main jet at the chamber inlet:

$$Re = \frac{\rho W_i d}{\mu} \quad (1)$$

where W_i is the main jet average axial velocity at the chamber inlet and ρ and μ are the working fluid density and dynamic viscosity, respectively. The experiments presented here were conducted at $Re = 38,000$ and $Re = 62,000$ corresponding to $W_i = 7.5 \frac{\text{m}}{\text{s}}$ and $W_i = 12.3 \frac{\text{m}}{\text{s}}$ respectively.

2.2 Micro-jet actuation

Active control is performed using twelve micro-jets with a diameter $\frac{d_{cj}}{d} = 0.1$ around the circumference of the main jet (see Figure 1(b)). The micro-jets injected water through twelve micro channels using twelve on/off automotive fuel injectors (INJL48, Standard Motor Products). The nominal flow rate of the fuel injectors is 492 ml/min for a pressure difference of 689 kPa (100 psi) across the injector resulting in a micro-jet velocity of 40 m/s and this remained constant for both Reynolds conditions. The ratio of the velocity of the micro-jet to the main jet ($\frac{W_{cj}}{W_i}$) is 5.33 and 3.25 for $Re = 38,000$ and $Re = 62,000$ respectively. Simultaneous use of three of twelve micro-jets in a configuration as shown in Figure 2, was found to be effective in controlling the precessing jet and as such this pattern is used in all experiments presented in this study. Three successive injectors ($n=3$, where n is the number of injectors that are actuated simultaneously) are always firing and this pattern rotates completely (i.e. 360°) around the jet axis with a frequency ($f = 5$ Hz) in clockwise (CW) or

counterclockwise (CCW) direction. This actuation frequency was selected being near the natural frequency of precession and having a high probability of precession (Madej et al, 2011; Babazadeh, 2011). The injectors are numbered from 1 starting at the positive Y axis and increasing in the CW direction. So the successive pattern (of firing injectors) for CW actuation is:

...,1-2-3, 2-3-4, 4-5-6 ...

and for CCW actuation:

...,1-2-3, 12-1-2, 11-12-1 ...

while the rest of the injectors are turned off. The frequency is defined based on the period which takes this pattern rotates a full cycle (i.e. 360°). Under these conditions, each injector is open for 50 ms.

The strength of actuation comparing to the main flow can be evaluated using momentum ratio (R_m) which is defined by Equation 2:

$$R_m = \frac{\sum_{i=1}^n W_{cj,i}^2 d_{cj,i}^2}{W_i^2 d^2} \quad (2)$$

where having three simultaneously firing injectors (i.e. $n = 3$) results in $R_m = 0.85$ and $R_m = 0.32$ for $Re = 38,000$ and $Re = 62,000$ respectively.

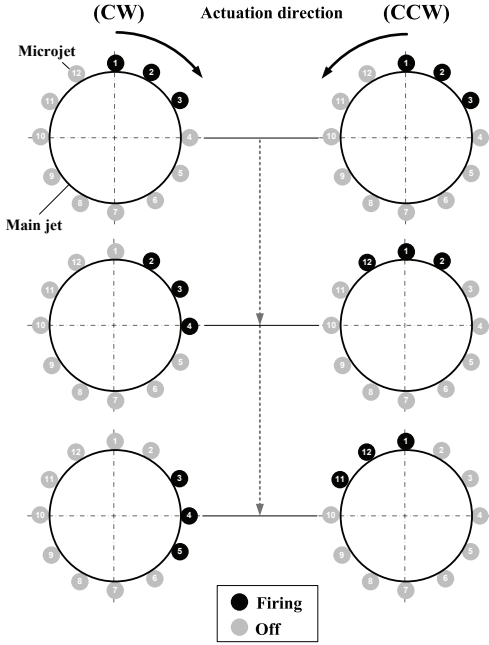


Fig. 2: The firing pattern of the injectors in CW and CCW actuation when three injectors fire simultaneously. This pattern rotates around the jet axis with the frequency of 5 Hz.

2.3 Pressure measurement

To observe the behavior of the precessing jet 4 pressure taps are located near the exit plane of the chamber as shown in Figure 1. These taps are located on the X and Y axes for a coordinate system defined looking directly back into the chamber from the exit. The pressure taps are connected to a pressure transducer (DP15, Validyne with a diaphragm range of 2 psi) and the transducer voltage is sampled at 3 kHz. The pressure sensors are calibrated in the range ± 14 kPa (± 2.0 psi) with an increment of 1.4 kPa (0.2 psi). The axial velocity W (aligned with the Z axis) at the location of the pressure ports is the largest velocity component and is largely responsible for the dynamic pressure captured by the four pressure probes at the chamber lip.

2.4 Velocity measurement with stereo-PIV

Detailed flow behavior of the precessing jet can be revealed by investigating its velocity vector field at the nozzle exit. Due to the three dimensionality of the precessing jet, stereoscopic particle image velocimetry (stereo-PIV) is chosen to obtain three components of the velocity field in a two dimensional ($X - Y$) plane just downstream of the chamber exit. Normally for stereo-PIV the light sheet is aligned with the maximum velocity component as an in-plane velocity component and strong out-of-plane velocities are avoided. Here the axial velocity W is the largest velocity component but is perpendicular or out-of-plane to the laser sheet. Therefore, unlike the conventional stereo-PIV setup, a camera arrangement as shown in Figure 3 is used to capture the velocity field at the chamber exit plane. A similar arrangement has been used (Van Doorne and Westerweel, 2007) to study laminar, transient and turbulent pipe flow using stereo-PIV. Figure 3 illustrates the stereo-PIV setup with respect to the tank and the plenum.

Table 1: Test conditions

Variable	value
Inlet nozzle diameter	$d = 5.08$ mm
Chamber diameter	$D = 25.4$ mm
Chamber length ratio	$\frac{L}{D} = 2.5$
Reynolds number ($\times 1000$)	$Re_D = 38$ and 62
Passive control	without center body
Actuation frequency	$f = 5$ Hz
Actuation pattern (number of simultaneously firing injectors)	3
Actuation direction	CW and CCW

The flow is initially seeded by $18 \pm 2 \mu\text{m}$ hollow glass non-porous spheres (60P18, Potters Industries) with a density of $0.6 \pm 0.05 \frac{\text{g}}{\text{cc}}$. The selection of seeding particles is a trade-off between improving laser light scattering by increasing particle size and decreasing velocity lag by using smaller particles. The particle type used in water in this research relatively meets both criteria (Melling, 1997; Raffel et al, 2007). To illuminate the particles, a dual-cavity Nd:YAG laser (PIV-400-10, Spectra Physics) is used. This laser delivers up to 400 mJ/pulse at a frequency-doubled output wavelength of 532 nm and an operating frequency (repetition rate) of 10 Hz. As shown in the top-view of Figure 3, images are collected using two dual frame cameras (Imager Pro X 4M, LaVision GmbH) which are mounted on a three dimensional traverse (Feed Axis LES5, Isel-Germany). These cameras have a resolution of 2048×2048 pixels and a dynamic range of 14-bits. The cameras are equipped with a 105 mm lens ($f/2.8$ EX DG Macro, SIGMA) with Scheimpflug adapters. The cameras are located at a downstream distance from the chamber exit of 0.32 m and image the flow at 16° (Camera#1) and 14° (Camera#2) with respect to the chamber axis (see Figure 3-top view).

To calibrate the imaged region, a 3-D (two level) calibration plate with dimensions of $106 \times 106 \times 12$ mm (Target Type 11, LaVision GmbH) is mounted in front of the nozzle in the plane of the laser sheet. Initially, a pinhole model was used to calculate the cameras physical parameters. A 3rd order polynomial is used to provide a robust calibration mapping due to the distortion in this optical arrangement. The average deviation of the dewarped mark positions on the target is 0.3 pixel for both cameras. The use of a self-calibration approach (Wieneke, 2005) decreases this value to less than 0.05 pixel.

The plenum is positioned the centerline of the tank such that the exit lip is $46d$ away from the end of the tank. Recent work (Madej et al, 2011) using the same plenum-nozzle configuration in the same flow tank showed that the presence of the free surface and side walls had a negligible effect on the decay of an axisymmetric jet. The same study also showed the close proximity of the end wall as shown in Figure 3-side view had a negligible effect of the precession characteristics of a precessing jet nozzle for several different chamber lengths. This was shown to be due to the rapid decay of the precessing jet downstream of the chamber.

To avoid reflection of the laser sheet by the chamber and chamber lip, a small gap (~ 4 mm) between the light sheet and the exit plane of the lip is used (see Figure 3-the expanded view). The light sheet itself had a thickness of 4 mm to allow capturing of the out-of-

plane component. The optimal time step between laser pulses is found to be 80 ms, for low Reynolds number cases and 55 ms for the high Reynolds number cases.

Collected images were processed using a multi-pass, box off-set cross correlation approach to calculate the velocity vector field. Two-passes with large window size (128×128 pixel with 75% overlap) followed by three-passes with a small window size of (64×64 pixel with 75% overlap) was used. The velocity vector field is further processed with a median filter which replaces each vector with the median value of all surrounding vectors (Babazadeh, 2011). The final vector field is further smoothed with a 3×3 smoothing filter to help resolve the bulk details of the flow. The final correlation size used was 64×64 pixel. These equates to the determination of the local flow velocity vector over a region of 1.1×1.1 mm. This is the in plane resolution of the vector measurement. The out-of-plane velocity is averaged over the thickness of the light sheet which was 4mm. This was necessarily larger because of the orientation of the light sheet to capture the large out-of-plane component.

Image capture and storage of up to 1 Hz is possible with this stereo-PIV hardware. Since a transient study of this flow requires a sampling rate of at least 100 Hz, as an alternative, a phase-locked imaging technique was used. A phased-lock stereo-PIV measurement system requires a trigger signal from the periodically forced flow which varies in phase about the forcing period. Possible trigger signals are the actuation input to the micro-jet solenoid injectors or the measured pressure signal output at the chamber exit. An example of employing the pressure signal to trigger the PIV system is introduced in (Wong et al, 2008). For this study the trigger of each of the twelve injectors is chosen and provides twelve phases for phase-locked stereo-PIV. To take care of any possible asymmetry in the flow, each of the twelve injectors are individually used to trigger stereo-PIV system within different experiments. Therefore, 48 tests ($12 \times 2 \times 2 = \text{trigger} \times \text{Re} \times \text{actuation direction}$) are conducted for conditions listed in Table 1 and 100 images are collected to generate phase averaged results which takes 100 [s] to operate the test.

3 Determining jet location from pressure measurement

The chaotic nature of the precessing jet makes it difficult to use conventional signal processing tools such as a Fourier transform or a cross correlation approach to study the frequency and jet direction characteristics of the precession phenomenon using data from the

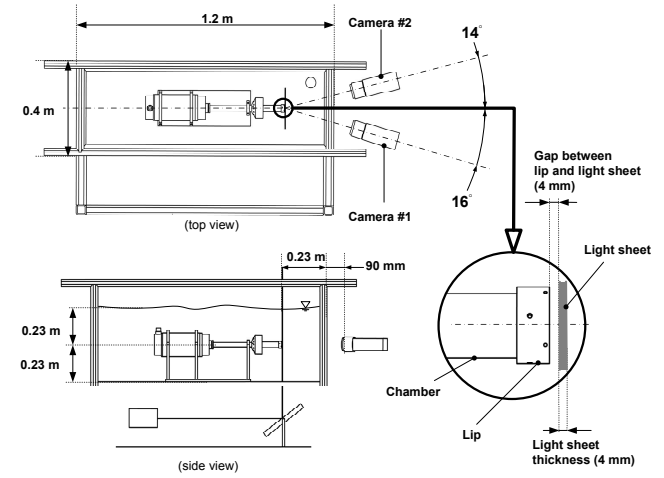


Fig. 3: A schematic view of the experimental set-up showing the arrangement of the stereo-PIV cameras with the containing tank, jet plenum and precessing nozzle.

pressure signals (Babazadeh, 2011). Fourier transform analysis of the pressure signals results in a noisy continuous spectra signature over a limited range of frequencies which can be an indicator of the chaotic nature of the flow (Moon, 1992). To use a cross correlation approach to analyze the pressure response of the precessing jet flow an appropriate window size for the signals is needed. This was found to be impractical since a large window size decreases the temporal resolution of the results while a small window does not distinctly capture the precession. This is partially attributed to the quasi-flapping motion of the precessing jet (regime 2) in which the jet passes (jumps) over a pressure probe without being captured by the corresponding pressure sensor.

An alternative approach to study the motion of a precessing jet is to determine a measure of the high velocity region of the jet at the chamber exit. Being able to determine a measure of the jet high velocity region using four pressure probes at the chamber exit allows for real-time monitoring of the precession characteristics. To accomplish this in the present work, a phase plane at the chamber exit is constructed by mapping the pressure data in a plane made up of a y axis, the difference between first and third sensors ($J_y = p_1 - p_3$) versus an x axis, the difference between second and fourth sensors ($J_x = p_2 - p_4$), as shown in Figure 4. The four pressure signals are simultaneously sampled in time and mapped onto the phase-plane shown at each sample instant. A radius and phase can be determined for each of these points as shown in Figure 4.

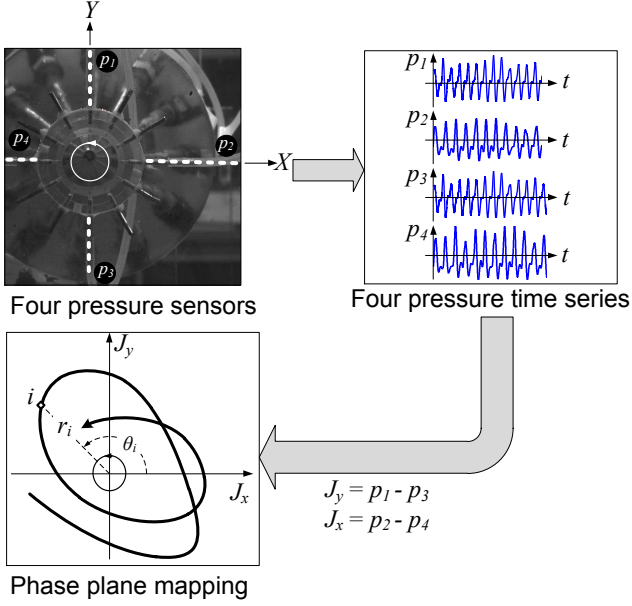


Fig. 4: An image of the location of four pressure probes on the periphery of the chamber with a representative pressure signal. A phase-plane representation of the relative location of jet high velocity region with respect to the probe locations over time is shown in the schematic view; the direction of the curve at the phase plane shows increasing time.

The phase plane used here is partially motivated by the concept of a *return map* found in chaos analysis. A description of chaotic motion in confined jet flows is given in (Ng, 1992). A more detailed study on chaotic behavior of an excited axisymmetric jet which resulted in a phase diagram depicting flow states with respect to some actuation (Broze and Hussain, 1994, 1996). In addition, the concept of a limit cycle has been used to study the transient nature of the precessing jet by plotting in-plane velocity components in a Cartesian coordinates (Guo et al, 2001).

An example of phase plane curve mapping which maintains the same (CW/CCW) rotation defined earlier is shown in Figure 4. The radius of this curve is interpreted as a measure of radial distance of the jet high velocity region from the chamber axis. That this trajectory mimics the trajectory of the high velocity region of the precessing jet at the chamber exit is assumed and will be confirmed later using stereo-PIV measurements.

The actuation signal is used to sample pressure data on the phase plane that correspond to stereo-PIV images (see Figure 5). For multiple images (100) these pressure points are mapped into the phase plane as shown in Figure 5 and the centroid is calculated to determine the average location of the high speed region of

the jet. The coordinates of the centroid ($J_{x,c}$ and $J_{y,c}$) shown in Figure 5 is calculated using:

$$J_{x,c} = \frac{\sum_{i=0}^N J_{x,i}}{N}, J_{y,c} = \frac{\sum_{i=0}^N J_{y,i}}{N} \quad (3)$$

where N is the number of phase-locked pressure data shown in Figure 5. This centroid will be used later for comparison with the actual location determined using stereo-PIV.

A two dimensional histogram of all 100 triggered pressure data in the phase plane is calculated such that the probability of the precessing jet location is indicated by an intensity of colour. All twelve trigger points at both Reynolds number and actuation directions are combined into a single figure as shown in Figure 6. The small circles around the main jet region represent the position and actuation of the microjets. These would normally overlap, but have been shown here with overlap removed for clarity. Each colour represents an experiment based on one of the twelve trigger states with the corresponding colour marking the three active micro-jet actuators. The distribution of the location of the jet maximum velocity shown in the different colour regions for $Re = 38,000$, in Figures 6(a) and 6(b), are relatively distinct while the distributions for $Re = 62,000$ in Figures 6(c) and 6(d) overlap each other. Moreover, comparing Figure 6(a) and (b) (low Reynolds number) with Figure 6(c) and (d) (high Reynolds number) shows that by increasing Reynolds number, the dynamic pressure measured in all probes increases which results in an increase in the radius of the pattern shown in Figure 6.

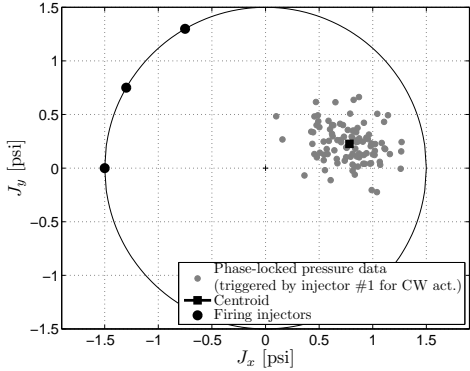


Fig. 5: The phase plane representation of the phase-locked pressure data and their centroid corresponding to injectors 11 and 12 for $\frac{L}{D} = 2.5$, $Re=62,000$ in the CW actuation with $f=5$ Hz. Refere to Figure 4 for the defintions of J_x and J_y .

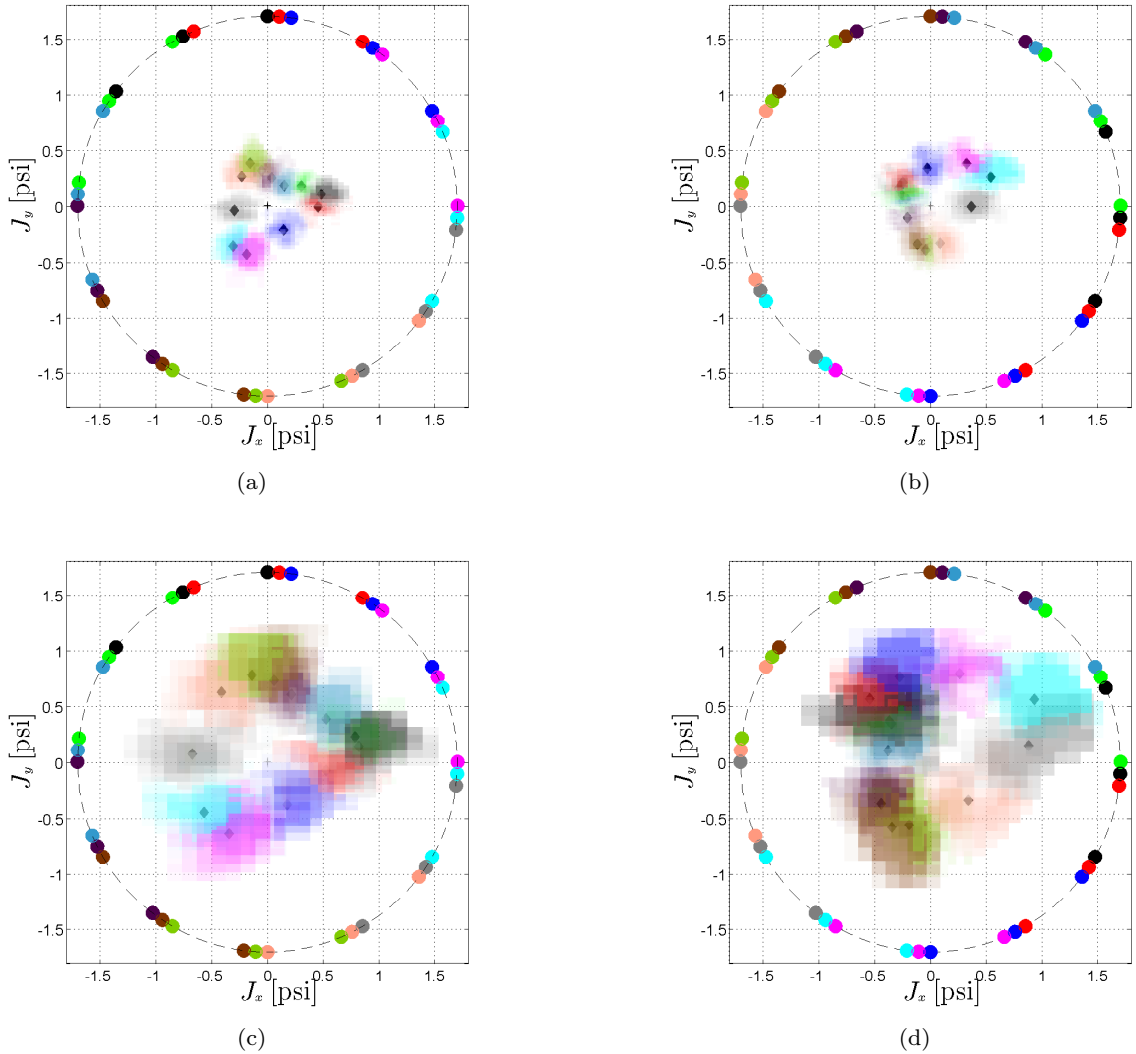


Fig. 6: The phase plane representation of the phase-locked pressure data and their centroid for all triggered microjets. Each colour represents a data set of 100 individual samples collected with a different trigger. For example, in (a): the red colour corresponds to a test with microjets 12, 1 and 2 actuated and the same colour inside the jet depicts the probability of finding the jet inside the region limited with the large circle. With decreasing probability, the colour fades to white (i.e. the probability of finding the jet for that actuation in white regions is zero). Data for $\frac{L}{D} = 2.5$, actuation frequency (f) of 5 Hz at (a) $Re=38,000$ in CW actuation, (b) $Re=38,000$ in CCW actuation, (c) $Re=62,000$ in CW actuation and (d) $Re=62,000$ in CCW actuation.

The results shown in Figure 6 highlight that in each of the four cases, the jet follows a unique path. This could be expected to be circular if the jet follows the actuation faithfully and the circular shape of the chamber as it passes through the exit plane of the nozzle. However, in all cases the path of the high velocity region of the jet is only near-circular and can possibly be attributed to asymmetries in the nozzle configuration due to manufacturing or slight differences in flow rates in the twelve micro-jets. Effectiveness of the ac-

tuation can be interpreted from the distribution of the collected signals. For both cases at $Re = 38,000$ the distribution is smaller than for the $Re = 62,000$ cases. This indicates that actuation is more effective at manipulating the jet position for $Re = 38,000$ than at $Re = 62,000$, perhaps due to the lower relative micro-jet momentum (the micro-jet flow rate is similar for both cases while momentum of the main jet increases with Reynolds number). The effect of actuation direction is also shown in Figure 6. The pattern of the lo-

cation of the maximum jet velocity in the phase plane is similar for the two Reynolds number cases investigated but different for the direction of actuation. This can most likely be attributed to slight asymmetries in the nozzle configuration. Comparing CW and CCW actuation at $Re = 62,000$ (Figures 6(c) and 6(d)) shows that there is more overlap in the CCW than in the CW case. This indicates that the CW direction is the preferred direction of this particular nozzle configuration. However, the actuation system is capable of affecting the direction of the flow in both directions.

4 Stereo-PIV measurement of axial velocity at the chamber exit

An example of an instantaneous velocity flow field for one trigger state at $Re = 62,000$ with CW actuation is shown in Figure 7. The flow is observed upstream looking along the jet axis into chamber from the outside. Added to the image is a solid black circle and a “+” representing the chamber exit wall the center of the chamber. The surrounding injection points for actuation are also include and the injectors that are actuated for this case are highlighted with solid circles. The instantaneous outflow velocity w of one image is depicted with the colourmap in Figure 7(a). This is the flow out-of-plane of the laser sheet of the stereo-PIV system and is the main velocity component of the jet. The corresponding transverse or in-plane instantaneous velocity field is shown in 2D vector map in Figure 7(b). This field shows the large-scale structure of the precessing jet exiting the chamber with a strong radial component. Injection of secondary flow through the actuation micro-jets pushes the main jet to the opposite side of the chamber. This wall jet interacts with the lip at the chamber exit which deflects the jet across chamber centerline resulting in the strong radial component of the jet as seen in Figure 7(b). As the measurement plane is downstream from the nozzle exit, a radial component of the jet outside the range of the chamber is also observed.

The one hundred phase-locked instantaneous flow fields collected for each test point are used to determine phase average and RMS velocity fields. Figure 8(a) and 8(b) illustrate the average (\bar{W}) and RMS (\bar{w}') outflow jet velocity at $Re = 62,000$ for the trigger state where the firing injectors are at the bottom-left of the nozzle inlet with CW actuation. These results show that there is a correlation between the phase of jet centroid and actuation phase. For example, when the firing injectors are located at the bottom-left side as shown in Figure 8(a), the precessing jet tends toward the opposite side. This figure also shows entrainment of fluid into

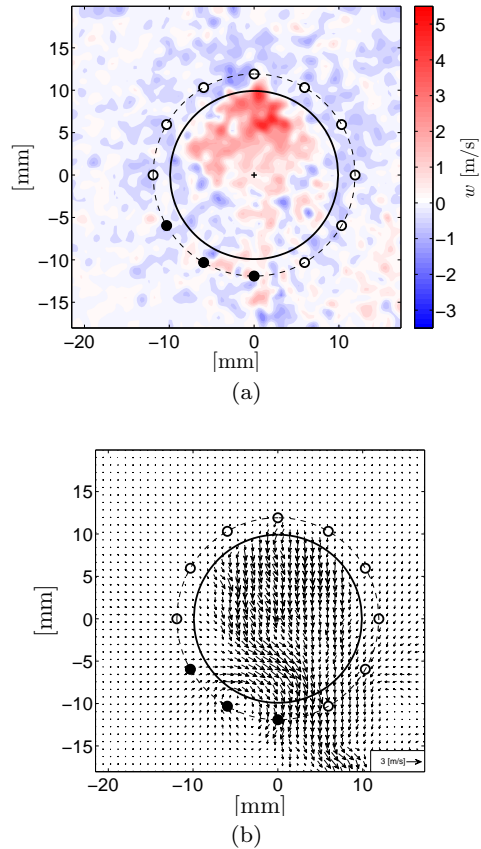


Fig. 7: Phase-locked instantaneous (a) outflow (out-of-plane) velocity (b) transverse (in-plane) velocity vector field of a chamber with a length ratio $\frac{L}{D} = 2.5$ at $Re=62,000$ with CW actuation, triggered by injector 10.

the chamber. A similar behavior is observed in all trigger cases. The RMS velocity field shown in figure 8(b) maps a high fluctuating component of the outflow velocity onto the main jet region and seen in figure 8(a). This indicates that there is a large fluctuation in the magnitude and location of the jet within the sample set however on average the position of the bulk jet flow is relatively uniform.

For comparison purposes, experiments without actuation are also performed and since there is no actuation images are taken at a random phase of the precessing jet. In particular, 1000 images were taken randomly without actuation (and therefore no trigger) at each of $Re = 38,000$ and $Re = 62,000$. A conditional averaging method was used to find the centroid of the high velocity region in the jet for each image and allow rotation of the velocity field about the nozzle axis to allow pseudo-phase averaging to occur (Madej, 2010; Madej et al. 2011).

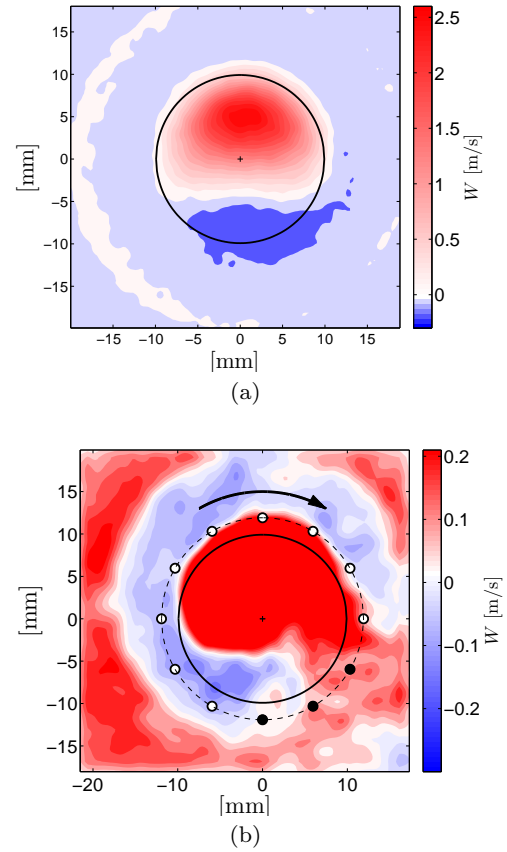
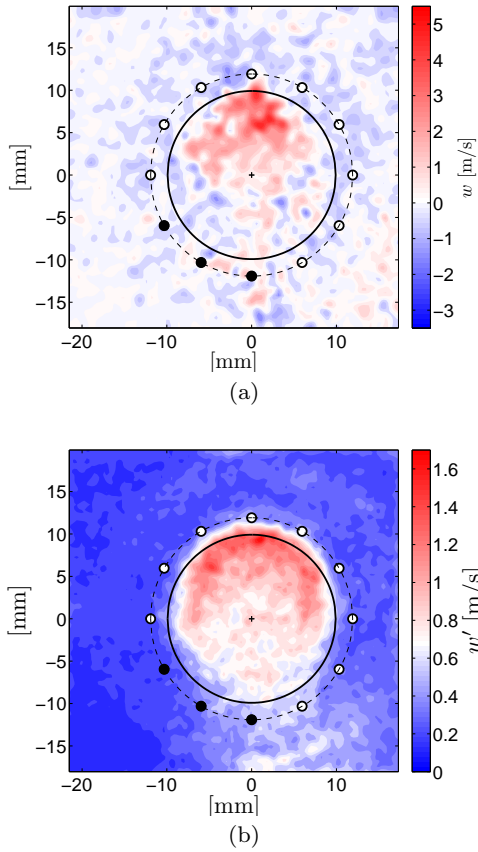


Fig. 8: Phase-locked (a) average (b) RMS outflow velocity component for $\frac{L}{D} = 2.5$ at $Re=62,000$ with $f = 5$ Hz CW actuation and phased-locked by injector 10.

The conditionally averaged outflow velocity (W) at $Re = 62,000$ for a chamber length of $\frac{L}{D} = 2.5$ is shown in Figure 9(a). This reveals that the un-actuated precessing jet has a relatively symmetrical kidney-bean shaped region described by the outflow. In comparison images of the outflow of the micro-jet actuated precessing jet shown in Figure 9(b) for CW and Figure 9(c) for CCW, it is apparent that the actuation changes the kidney-bean cross sectional shape of the precessing jet to a paisley shape (or a twisted teardrop). The direction of precession and actuation is shown with an arrow for the CW and CCW actuation directions in Figure 9(b) and 9(c). The narrow side of the high velocity region indicates the leading edge while the round side of the twisted teardrop is the trailing part of the precessing jet. Compared to the case without actuation, the micro-jet actuation forces the flow to follow the actuation direction which also distorts the symmetry of the outflow velocity of the precessing jet shape at the chamber exit.

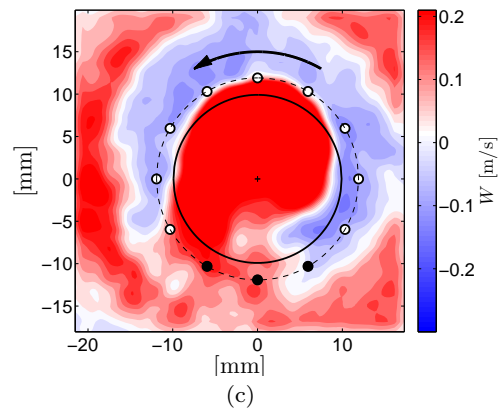


Fig. 9: (a) Conditionally averaged outflow velocity for $\frac{L}{D} = 2.5$ at $Re=62,000$ without actuation (b) Spatially smoothed phase-locked average outflow velocity for $f = 5$ Hz CW actuation and phased-locked by injector 8 (c) $f = 5$ Hz CCW actuation and phased-locked by injector 5.

5 Determination of jet location from stereo-PIV and pressure measurements

To determine how well the boundary measurement method using pressure transducers can resolve the position of

the jet, a comparison between the location of the high velocity region of the jet in the phase plane as determined from the pressure measurements and the stereo-PIV measurements is performed. A centroid-of-outflow-velocity approach based on phased average stereo-PIV images is used to determine the precessing jet location (Madej, 2010; Madej et al, 2011). The phase of the centroid for both techniques relative to the trigger position is defined in Figure 10. The injection line is defined as a reference phase, φ , of the location of the actuation and is located on the opposite side of the center of the active injectors as shown in Figure 10. Phase, θ , is defined as the angle between the jet centroid and the x -axis. The angle β , is the phase difference between the centroid phase angle, θ , and the injection phase, φ . The figure shows that there is a phase difference between the results. The magnitude of this phase lag relative to the injection line is defined as β_{PIV} or β_p in Figure 10.

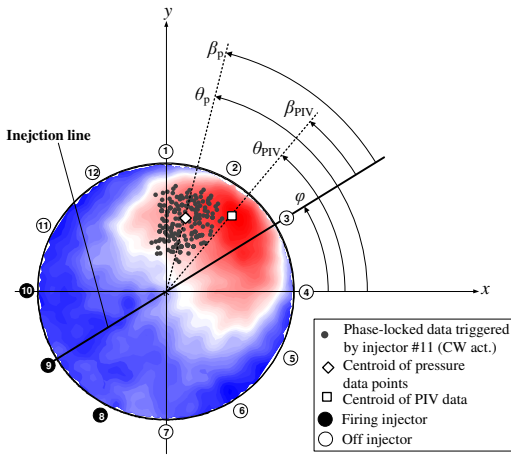


Fig. 10: The definition of phase and lag between the injection line and the centroid of jet obtained by PIV data and pressure measurement.

The injector phase, φ and the centroid phase values based on both pressure data, θ_p , and stereo-PIV, θ_{PIV} are plotted in Figure 11(a) and (b). Both pressure and stereo-PIV measurement methods show similar phase trends indicating that the precessing jet always lags behind the injection line with respect to the actuation direction. A comparison of the average phase lag difference between stereo-PIV and pressure data for all twelve injector phases is defined as $\Delta\beta = \sum_{i=1}^{12} (\beta_{\text{PIV}_i} - \beta_{p_i})/12$, and is listed in Table 2.

The average phase difference of $\Delta\beta$ between stereo-PIV and pressure data is shown in schematic view in

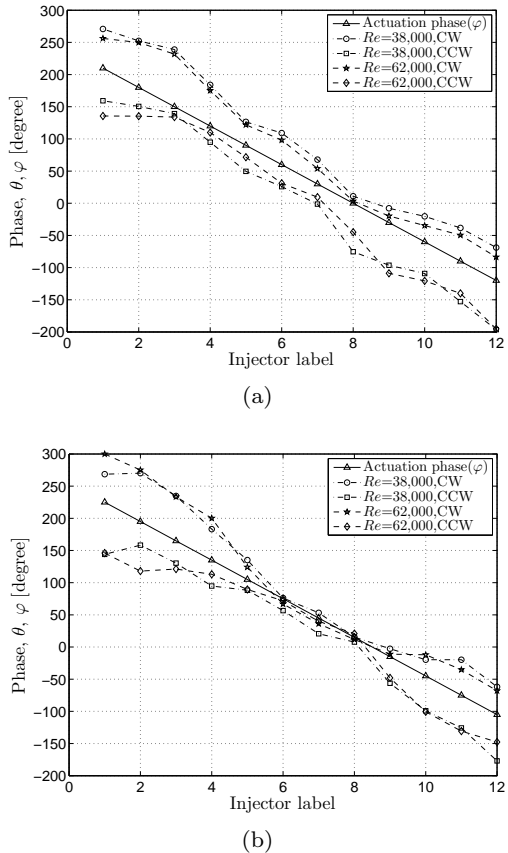


Fig. 11: The phase of the precessing jet centroid for $\frac{L}{D} = 2.5$ and $f = 5$ Hz, comparing with the phase of injection line at $Re=38,000$ and $Re=62,000$ for CW and CCW actuation obtained based on (a) pressure signals (b) stereo-PIV images.

Table 2: Precessing jet phase at the chamber exit ($\Delta\beta = \beta_{\text{PIV}} - \beta_p$), average over all 12 injector phases.

Re	$\Delta\beta$ CW Act.	$\Delta\beta$ CCW Act.
38,000	-30°	21°
62,000	-21°	23°

Figure 12. This indicates that the pressure data estimation lags the stereo-PIV estimate by $\Delta\beta \approx 20 - 30^\circ$. The relatively simple relation between the high velocity centroid of the precessing jet determined by the pressure sensors and that of stereo-PIV is of great interest as it indicates that the pressure sensors can be used as a measure of the location of the precessing jet. Thus, four pressure sensors located at the surface of the chamber are able to determine the location of the high velocity region of the precessing jet at the exit plane of the nozzle chamber. This is an important result since pressure sensors can easily be used in industrial flows

where stereo-PIV is impractical. The stereo-PIV system collects images at approximately 1 Hz that are phase locked to the micro-jet actuation but this sample rate is too slow for closed loop control of jet precession. However, the pressure signal response is substantially faster than the processing jet frequency which means that the pressure signals can be used in future real-time closed loop control. In addition, for active flow control, appropriate actuators are needed and for the precessing jet in the range of flow studied, the 12 micro jet actuators are effective in influencing the precession direction.

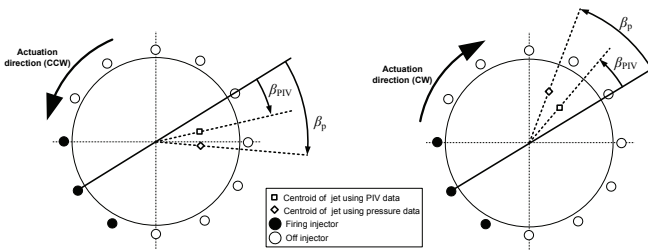


Fig. 12: The schematic representation of the centroid phase obtained by PIV and pressure data with respect to the injection line.

6 Conclusion

Twelve micro-jets mounted on the periphery of the nozzle inlet into a precessing jet chamber are used to actively control a precessing jet. The flow field is monitored using: four pressure signals at the chamber exit; and by three components of velocity using stereo-PIV on a plane just downstream of the chamber exit. A phase plane, made up by subtracting vertical pressure signals as the y axis and a subtracting horizontal pressure signals for x axis, is developed and found useful to extract information about the characteristics of jet precession. Phase-locked stereo-PIV measurement is used to verify that the pressure phase plane corresponds to the jet position determined by stereo-PIV. The results show that the phase of the center of the precessing jet estimated using the pressure sensors at the chamber exit lags about 20° - 30° behind the jet center determined by the stereo-PIV measurement. Thus for this flow system the pressure sensors can be used to estimate the jet precessing characteristics for future active flow control with feedback.

References

- Babazadeh H (2011) Active flow control of a precessing jet. Master's thesis, University of Alberta, URL <http://hdl.handle.net/10048/1636>
- Behrouzi P, Feng T, McGuirk J (2008) Active flow control of jet mixing using steady and pulsed fluid tabs. Proceedings of the Institution of Mechanical Engineers Part I: Journal of Systems and Control Engineering 222(5):381–392
- Broze G, Hussain F (1994) Nonlinear dynamics of forced transitional jets: periodic and chaotic attractors. Journal of Fluid Mechanics 263:93–132
- Broze G, Hussain F (1996) Transitions to chaos in a forced jet: Intermittency, tangent bifurcations and hysteresis. Journal of Fluid Mechanics 311:37–71
- England G, Kalt P, Nathan G, Kelso R (2010) The effect of density ratio on the near field of a naturally occurring oscillating jet. Experiments in Fluids 48(1):69–80
- Gad-el-Hak M (2006) Flow control, passive, active and reactive flow management. Cambridge University Press
- Guo B, Langrish T, Fletcher D (2001) Numerical simulation of unsteady turbulent flow in axisymmetric sudden expansions. J Fluids Eng 123:574–587
- Huerre P, Monkewitz P (1985) Absolute and convective instabilities in free shear layers. Journal of Fluid Mechanics 159:151–168
- King R, Mehrmann V, Nitsche W (2010) Active flow control a mathematical challenge. In: Grtschel M, Lucas K, Mehrmann V (eds) Production Factor Mathematics, Springer Berlin Heidelberg, pp 73–80
- Madej A (2010) The experimental investigation of the effect of chamber length on jet precession. Master's thesis, University of Alberta, URL <http://hdl.handle.net/10048/1253>
- Madej A, Babazadeh H, Nobes DS (2011) The effect of chamber length and reynolds number on jet precession. Experiments in Fluid (in press)
- Manias C, Balendra A, Retallack D (1996) New combustion technology for lime production. World Cement 27(12):34–39
- Melling A (1997) Tracer particles and seeding for particle image velocimetry. Meas Sci Technol 8:1406–1416
- Mi J, Nathan G (2009) Statistical properties of turbulent free jets issuing from nine differently-shaped nozzles. Flow, Turbulence and Combustion pp 1–24, article in Press
- Moon F (1992) Chaotic and fractal dynamics, an introduction for applied scientists and engineers. John Wiley & Sons, Inc.

- Nathan G (1988) The enhanced mixing burner. PhD thesis, University of Adelaide
- Nathan G, Hill S, Luxton R (1998) An axisymmetric nozzle to generate jet precession. *Journal of Fluid Mechanics* 370:347–380
- Nathan G, Mi J, Alwahabi Z, Newbold G, Nobes D (2006) Impacts of a jet's exit flow pattern on mixing and combustion performance. *Progress in Energy and Combustion Science* 32(5-6):496–538
- Newbold G (1998) Mixing and combustion in precessing jet flows. PhD thesis, University of Adelaide
- Ng K (1992) Chaotic motion in confined jet flows. In: ASME, AMD-Vol. 151, PVP-Vol. 247 Symposium on flow-induced vibration and noise
- Raffel M, Willert C, Wereley S, Kompenhans J (2007) Particle image velocimetry: A practical guide. Springer-Verlag
- Van Doorne C, Westerweel J (2007) Measurement of laminar, transitional and turbulent pipe flow using stereoscopic-piv. *Experiments in Fluids* 42(2):259–279
- Wieneke B (2005) Stereo-piv using self-calibration on particle images. *Experiments in Fluids* 39(2):267–280
- Wong C, Lanspeary P, Nathan G, Kelso R, O'Doherty T (2003) Phase-averaged velocity in a fluidic precessing jet nozzle and in its near external field. *Experimental Thermal and Fluid Science* 27:515–524
- Wong C, Nathan G, O'Doherty T (2004) The effect of initial conditions on the exit flow from a fluidic precessing jet nozzle. *Experiments in Fluids* 36:70 – 81
- Wong C, Nathan G, Kelso R (2008) The naturally oscillating flow emerging from a fluidic precessing jet nozzle. *Journal of Fluid Mechanics* 606:153–188